The choice of machine learning algorithms impacts the association between brain-predicted age difference and cognitive function

Supplementary Materials

Supplementary Methods

1. Cam-CAN neuroimaging acquisition

MRI data were acquired on a 3T Siemens TIM Trio scanner with a 32-channel head coil, using a T1-weighted, 3D MPRAGE sequence with the following parameters: TR/TE/TI = 2250/2.99/900 ms, voxel size = 1 mm isotropic, flip angle = 9°, FOV = 256 × 240 × 192 mm^3, duration of acquisition = 4 min 32 s. Two-shell DTI datasets were acquired using a twice-refocused diffusion pulsed-gradient spin-echo (SE) echo-planar imaging (EPI) sequence with the following imaging parameters: TR/TE = 9100/104 ms, FOV = 192 × 192 mm^2, voxel size = 2 mm isotropic, 66 axial slices using 30 directions with b = 1000 s/mm^2, 30 directions with b = 2000 s/mm^2, and 3 images with b = 0 s/mm^2.

2. Processing of the structural and diffusion MRI data

The T1-weighted images were downloaded from the Cam-CAN repository and processed locally. Cortical reconstruction and volumetric segmentation of the structural dataset were conducted using FreeSurfer image analysis suite (version 6.0) which is documented and freely available (http://surfer.nmr.mgh.harvard.edu/). Processing included removal of non-brain tissue using a hybrid watershed/surface deformation procedure,[1] segmentation of the subcortical white matter and deep gray matter volumetric structures,[2, 3] intensity normalization,[4] tessellation of the boundary of gray matter (GM) and white matter (WM), automated topology correction[5] and surface deformation following intensity gradients to optimally place the gray/white and gray/cerebrospinal fluid (CSF) borders at the location where the greatest shift in intensity defines the transition to the other tissue class.

Diffusion image processing was performed using FSL (version 6.0), which is a part of the Functional Magnetic Resonance Imaging of the Brain (FMRIB) Software Library. Eddy currents and movement were corrected using FSL's *eddy* tool. Fractional anisotropy (FA), mean (MD), axial (AD), and radial diffusivity (RD) maps were computed by fitting a tensor model to the corrected DTI data using FSL's *dtifit* tool. All diffusivity maps were non-linearly normalized to the Montreal Neurological Institute (MNI) space using FSL's FMRIB58_FA template as the reference target.

3. Image feature extraction

Area parcellation based on the Desikan-Killiany atlas,[3, 6] and the probabilistic atlas for subcortical regions.[2] was implemented in Freesurfer 6.0 to extract 153 features (68 surface area measures, 68 cortical thickness measures, 16 subcortical volumes, and total intracranial volume) (Supplementary Table S1). Regional measures of each diffusion metric (FA, MD, AD, RD) were extracted by using the John Hopkins University (JHU) parcellation atlas. This parcellation consists of 48 regional estimates of white matter tracts, resulting in a total of 192 regional white matter diffusion measures (Supplementary Table S1).

4. Quality assurance of structural and diffusion MRI data

Each structural and diffusion dataset was evaluated according to the publicly available protocol from the ENIGMA initiative (http://enigma.ini.usc.edu/) and using Qoala-T for the FreeSurfer segmentation.[7]

Supplementary Table S1. Definition of the neuroimaging measures	
Cortical thickness and surface area	
Caudal anterior cingulate cortex	Derived from cortical reconstruction using Freesurfer 6; left and right measures were considered separately
Caudal middle frontal gyrus	Derived from cortical reconstruction using Freesurfer 6; left and right measures were considered separately
Cuneus	Derived from cortical reconstruction using Freesurfer 6; left and right measures were considered separately
Entorhinal cortex	Derived from cortical reconstruction using Freesurfer 6; left and right measures were considered separately
Fusiform gyrus	Derived from cortical reconstruction using Freesurfer 6; left and right measures were considered separately
Inferior parietal lobule	Derived from cortical reconstruction using Freesurfer 6; left and right measures were considered separately
Inferior temporal gyrus	Derived from cortical reconstruction using Freesurfer 6; left and right measures were considered separately
Lateral occipital gyrus	Derived from cortical reconstruction using Freesurfer 6; left and right measures were considered separately
Lateral orbitofrontal gyrus	Derived from cortical reconstruction using

Supplementary Table S1. Definition of the neuroimaging measures	
	Freesurfer 6; left and right measures were considered separately
Lingual gyrus	Derived from cortical reconstruction using Freesurfer 6; left and right measures were considered separately
Medial orbitofrontal gyrus	Derived from cortical reconstruction using Freesurfer 6; left and right measures were considered separately
Middle temporal gyrus	Derived from cortical reconstruction using Freesurfer 6; left and right measures were considered separately
Parahippocampal gyrus	Derived from cortical reconstruction using Freesurfer 6; left and right measures were considered separately
Paracentral gyrus	Derived from cortical reconstruction using Freesurfer 6; left and right measures were considered separately
Pars opercularis	Derived from cortical reconstruction using Freesurfer 6; left and right measures were considered separately
Pars orbitalis	Derived from cortical reconstruction using Freesurfer 6; left and right measures were considered separately
Pars triangularis	Derived from cortical reconstruction using Freesurfer 6; left and right measures were considered separately
Pericalcarine gyrus	Derived from cortical reconstruction using Freesurfer 6; left and right measures were considered separately
Postcentral gyrus	Derived from cortical reconstruction using Freesurfer 6; left and right measures were considered separately
Posterior cingulate cortex	Derived from cortical reconstruction using Freesurfer 6; left and right measures were considered separately
Precentral gyrus	Derived from cortical reconstruction using Freesurfer 6; left and right measures were considered separately
Precuneus	Derived from cortical reconstruction using Freesurfer 6; left and right measures were considered separately
Rostral anterior cingulate cortex	Derived from cortical reconstruction using Freesurfer 6; left and right measures were considered separately
Rostral middle frontal gyrus	Derived from cortical reconstruction using

Supplementary Table S1. Definition of the neuroimaging measures	
	Freesurfer 6; left and right measures were considered separately
Superior frontal gyrus	Derived from cortical reconstruction using Freesurfer 6; left and right measures were considered separately
Superior parietal lobule	Derived from cortical reconstruction using Freesurfer 6; left and right measures were considered separately
Superior temporal gyrus	Derived from cortical reconstruction using Freesurfer 6; left and right measures were considered separately
Supramarginal gyrus	Derived from cortical reconstruction using Freesurfer 6; left and right measures were considered separately
Frontal pole	Derived from cortical reconstruction using Freesurfer 6; left and right measures were considered separately
Temporal pole	Derived from cortical reconstruction using Freesurfer 6; left and right measures were considered separately
Transverse temporal gyrus	Derived from cortical reconstruction using Freesurfer 6; left and right measures were considered separately
Insula	Derived from cortical reconstruction using Freesurfer 6; left and right measures were considered separately
Subcortical volume	
Thalamus	Derived from segmentation using Freesurfer 6; left and right measures were considered separately
Hippocampus	Derived from segmentation using Freesurfer 6; left and right measures were considered separately
Caudate nucleus	Derived from segmentation using Freesurfer 6; left and right measures were considered separately
Nucleus Accumbens	Derived from segmentation using Freesurfer 6; left and right measures were considered separately
Pallidum	Derived from segmentation using Freesurfer 6; left and right measures were considered separately
Putamen	Derived from segmentation using Freesurfer 6; left and right measures were considered separately

Supplementary Table S1. Definition of the neuroimaging measures	
Amygdala	Derived from segmentation using Freesurfer 6; left and right measures were considered separately
Cerebellum	Derived from segmentation using Freesurfer 6; left and right measures were considered separately
Lateral ventricles	Derived from segmentation using Freesurfer 6
White matter integrity (fractional anisotropy, mean, axial, and radial diffusivity)	
Middle_cerebellar_peduncle	Derived from JHU atlas using FSL 6
Pontine_crossing_tract	Derived from JHU atlas using FSL 6
Genu_of_corpus_callosum	Derived from JHU atlas using FSL 6
Body_of_corpus_callosum	Derived from JHU atlas using FSL 6
Splenium_of_corpus_callosum	Derived from JHU atlas using FSL 6
Fornix	Derived from JHU atlas using FSL 6
Corticospinal_tract_R	Derived from JHU atlas using FSL 6; right measure was considered
Corticospinal_tract_L	Derived from JHU atlas using FSL 6; left measure was considered
Medial_lemniscus_R	Derived from JHU atlas using FSL 6; right measure was considered
Medial_lemniscus_L	Derived from JHU atlas using FSL 6; left measure was considered
Inferior_cerebellar_peduncle_R	Derived from JHU atlas using FSL 6; right measure was considered
Inferior_cerebellar_peduncle_L	Derived from JHU atlas using FSL 6; left measure was considered
Superior_cerebellar_peduncle_R	Derived from JHU atlas using FSL 6; right measure was considered
Superior_cerebellar_peduncle_L	Derived from JHU atlas using FSL 6; left measure was considered
Cerebral_peduncle_R	Derived from JHU atlas using FSL 6; right measure was considered
Cerebral_peduncle_L	Derived from JHU atlas using FSL 6; left measure was considered
Anterior_limb_of_internal_capsule_R	Derived from JHU atlas using FSL 6; right measure was considered
Anterior_limb_of_internal_capsule_L	Derived from JHU atlas using FSL 6; left measure was considered
Posterior_limb_of_internal_capsule_R	Derived from JHU atlas using FSL 6; right measure was considered
Posterior_limb_of_internal_capsule_L	Derived from JHU atlas using FSL 6; left measure was considered
Retrolenticular_part_of_internal_capsule_R	Derived from JHU atlas using FSL 6; right measure was considered

Supplementary Table S1. Definition of the neuroimaging measures	
Retrolenticular_part_of_internal_capsule_L	Derived from JHU atlas using FSL 6; left measure was considered
Anterior_corona_radiata_R	Derived from JHU atlas using FSL 6; right measure was considered
Anterior_corona_radiata_L	Derived from JHU atlas using FSL 6; left measure was considered
Superior_corona_radiata_R	Derived from JHU atlas using FSL 6; right measure was considered
Superior_corona_radiata_L	Derived from JHU atlas using FSL 6; left measure was considered
Posterior_corona_radiata_R	Derived from JHU atlas using FSL 6; right measure was considered
Posterior_corona_radiata_L	Derived from JHU atlas using FSL 6; left measure was considered
Posterior_thalamic_radiation_R	Derived from JHU atlas using FSL 6; right measure was considered
Posterior_thalamic_radiation_L	Derived from JHU atlas using FSL 6; left measure was considered
Sagittal_stratum_R	Derived from JHU atlas using FSL 6; right measure was considered
Sagittal_stratum_L	Derived from JHU atlas using FSL 6; left measure was considered
External_capsule_R	Derived from JHU atlas using FSL 6; right measure was considered
External_capsule_L	Derived from JHU atlas using FSL 6; left measure was considered
Cingulum_(cingulate_gyrus)_R	Derived from JHU atlas using FSL 6; right measure was considered
Cingulum_(cingulate_gyrus)_L	Derived from JHU atlas using FSL 6; left measure was considered
Cingulum_(hippocampus)_R	Derived from JHU atlas using FSL 6; right measure was considered
Cingulum_(hippocampus)_L	Derived from JHU atlas using FSL 6; left measure was considered
Fornix / Stria_terminalis_R	Derived from JHU atlas using FSL 6; right measure was considered
Fornix / Stria_terminalis_L	Derived from JHU atlas using FSL 6; left measure was considered
Superior_longitudinal_fasciculus_R	Derived from JHU atlas using FSL 6; right measure was considered
Superior_longitudinal_fasciculus_L	Derived from JHU atlas using FSL 6; left measure was considered
Superior_fronto-occipital_fasciculus_R	Derived from JHU atlas using FSL 6; right measure was considered
Superior_fronto-occipital_fasciculus_L	Derived from JHU atlas using FSL 6; left

Supplementary Table S1. Definition of the neuroimaging measures	
	measure was considered
Inferior_fronto-occipital_fasciculus_R	Derived from JHU atlas using FSL 6; right measure was considered
Inferior_fronto-occipital_fasciculus_L	Derived from JHU atlas using FSL 6; left measure was considered
Uncinate_fasciculus _R	Derived from JHU atlas using FSL 6; right measure was considered
Uncinate_fasciculus _L	Derived from JHU atlas using FSL 6; left measure was considered

Supplementary Table S2. Sample and demographic information for the Cam-CAN cohort used for brain age prediction

Cohort	Sample size	Males/Females	Age range (mean ± SD)
Datasets used in the training set			
Cam-CAN	500	249/251	54.40 ± 18.26
Hold-out test datasets			
Cam-CAN	101	50/51	54.38 ± 17.51

5. Cognitive function measures

We used seven cognitive measures that assess emotion processing, executive function, memory, and motor function obtained from the Cam-CAN repository. Emotional processing was measured using Ekman's emotion expression recognition test. Higher scores on Ekman's emotion expression test indicates greater recognition of facial expressions and emotions. Executive function was measured using 1) Cattell's fluid intelligence test, 2) the hotel test, and 3) a proverb comprehension task. Higher total scores on Cattell's fluid intelligence test across its four sub-tests indicate greater intelligence and mental control. Shorter times on each of the five trials of the hotel test indicate greater complex planning and multitasking ability. More proverbs correctly interpreted during the proverb comprehension test indicate greater executive function and abstraction ability. Memory was measured using the tip of the tongue (ToT) test. A greater proportion of ToT responses on the eponymous test indicates worse name recall and lexical production. Motor function was assessed using 1) a RT choice task and 2) a RT simple task. Slower mean reaction times on both the choice and simple tasks indicate worse response speed for actions requiring decision-making and automatic processing respectively.

Supplementary Table S3. Cam-CAN cognitive measures tested (7 variables)

Category	**Name of variable in the Cam-CAN database**	**Description**
Fluid intelligence	Cattell	Subject is given a multiple-choice exam on pen-and-paper. After, the RA calculates sub-scores and total score for an overall value.
Executive function	Hotel	Subject acts as a hotel manager performing 5 tasks. Subject must allocate 10 minutes equally; there is not enough time for completion. The ideal timing is 2 minutes per task. The time the subject needs to complete each task is recorded.
Executive function	Proverbs	Read, interpret, and explain 3 English proverbs. Score of 0 means no comprehension, 1 indicates partially correct (more literal), and 2 means fully correct (abstract).
Memory	ToT	Tip of the Tongue (TOT): Pictures of famous individuals (musicians, actresses, politicians, etc.…) are shown, and subject must say the person's name, "don't know" or "TOT" if they know the person's name

		but unable to retrieve it from memory.
Motor function	RT Simple (RTmean)	Participants view an image of a hand with blank circles on each finger while their hand rests on a response box. When the index finger is highlighted on screen, the subject must press with the corresponding finger as quickly as possible.
Motor function	RT Choice (RTmean_all)	
Emotion expression recognition	EkmanEmHex	View face and label emotion expressed (anger, disgust, fear, happy, sad, and surprise) where faces are morphs along axes between emotional expression. Average of anger, disgust, fear, happy, sad, and surprise

Supplementary Results

1. Brain regional regression weights

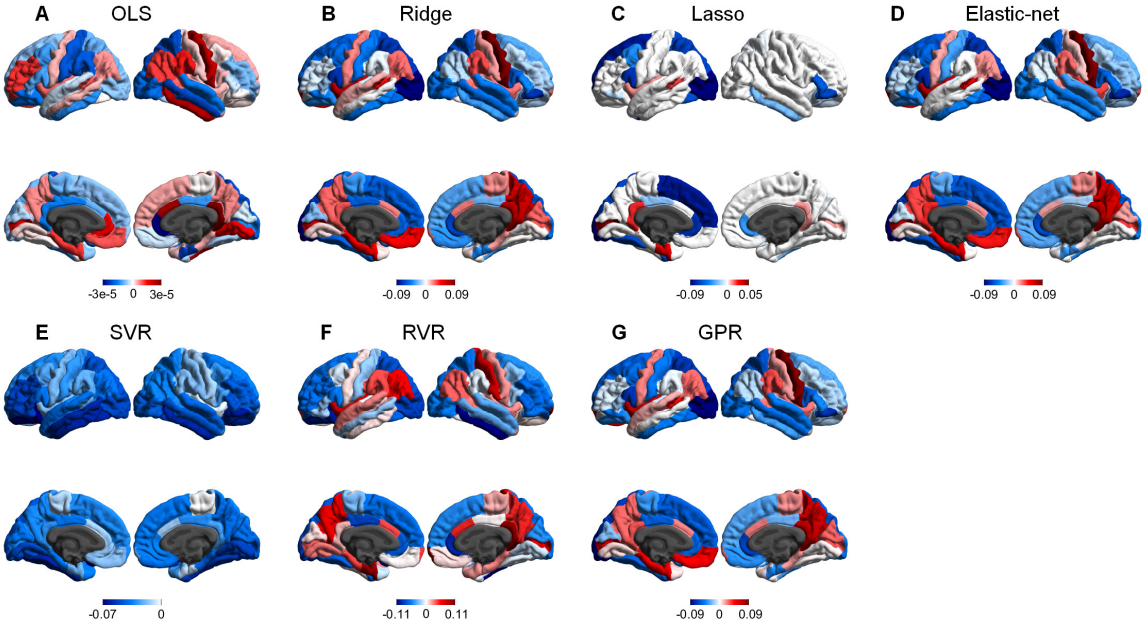

Supplementary Figure S1. Spatial map of regression weights for cortical surface area for brain-age prediction in Cam-CAN individuals in each of the seven algorithms. OLS: Ordinary least squares regression; Lasso: Least absolute shrinkage and selection operator; SVR: Support vector regression; RVR: Relevance vector regression; GPR: Gaussian process regression.

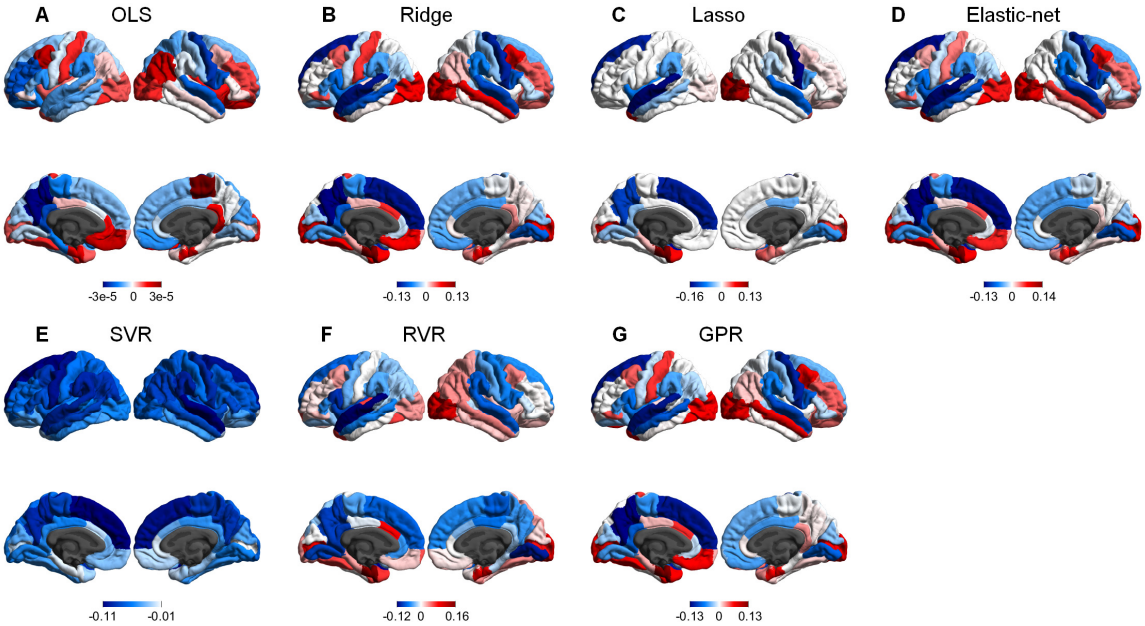

Supplementary Figure S2. Spatial map of regression weights for cortical thickness for brain-age prediction in Cam-CAN individuals in each of the seven algorithms. OLS: Ordinary least squares regression; Lasso: Least absolute shrinkage and selection operator; SVR: Support vector regression; RVR: Relevance vector regression; GPR: Gaussian process regression.

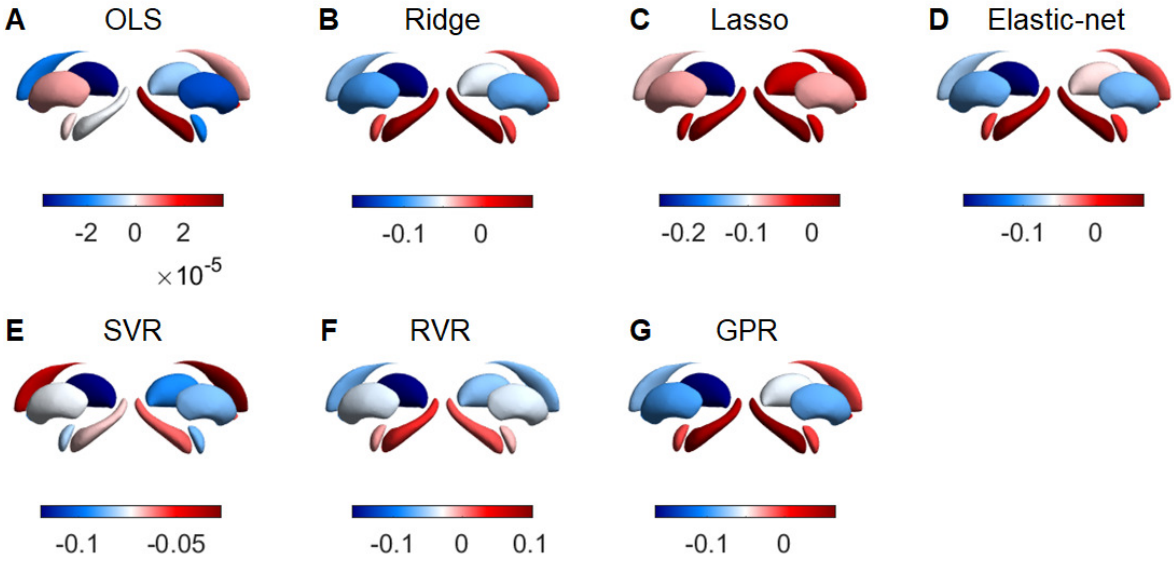

Supplementary Figure S3. Spatial map of regression weights for subcortical volume for brain-age prediction in Cam-CAN individuals in each of the seven algorithms. OLS: Ordinary least squares regression; Lasso: Least absolute shrinkage and selection operator;

SVR: Support vector regression; RVR: Relevance vector regression; GPR: Gaussian process regression.

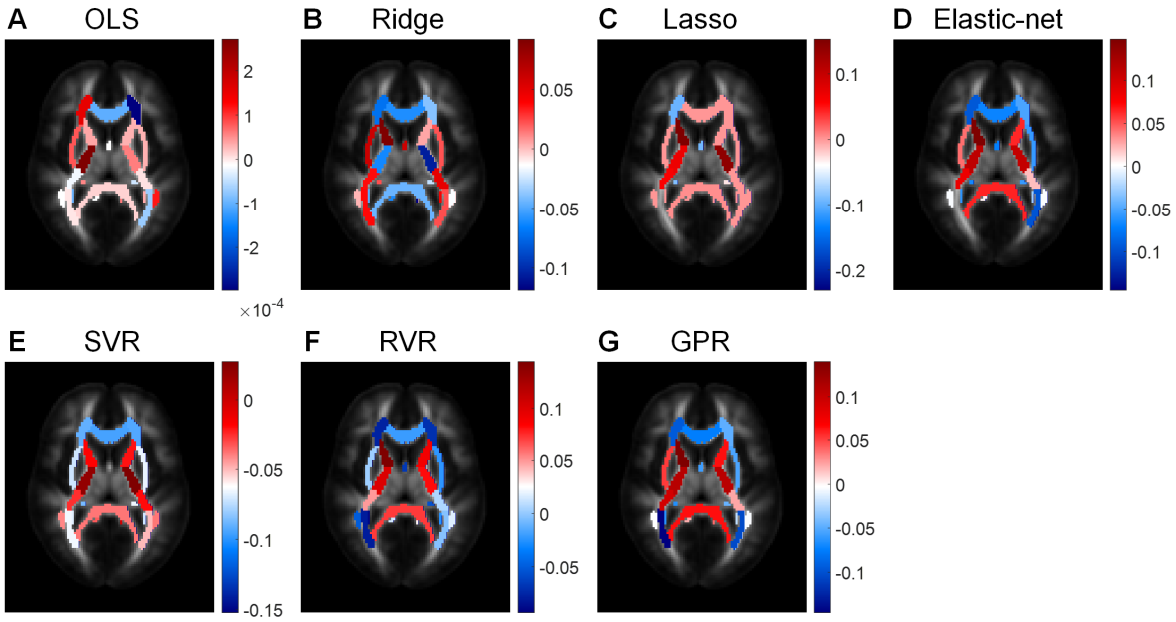

Supplementary Figure S4. A representative map of regression weights for fractional anisotropy for brain-age prediction in Cam-CAN individuals in each of the seven algorithms. OLS: Ordinary least squares regression; Lasso: Least absolute shrinkage and selection operator; SVR: Support vector regression; RVR: Relevance vector regression; GPR: Gaussian process regression.

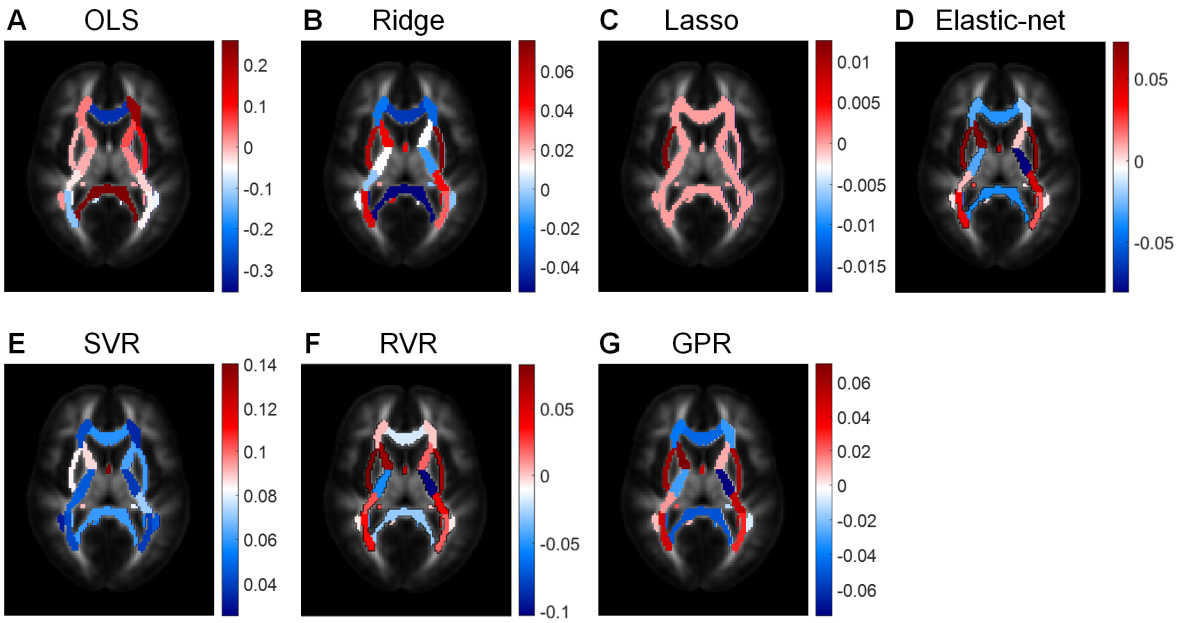

Supplementary Figure S5. A representative map of regression weights for mean diffusivity for brain-age prediction in Cam-CAN individuals in each of the seven algorithms. OLS: Ordinary least squares regression; Lasso: Least absolute shrinkage and selection operator; SVR: Support vector regression; RVR: Relevance vector regression; GPR: Gaussian process regression.

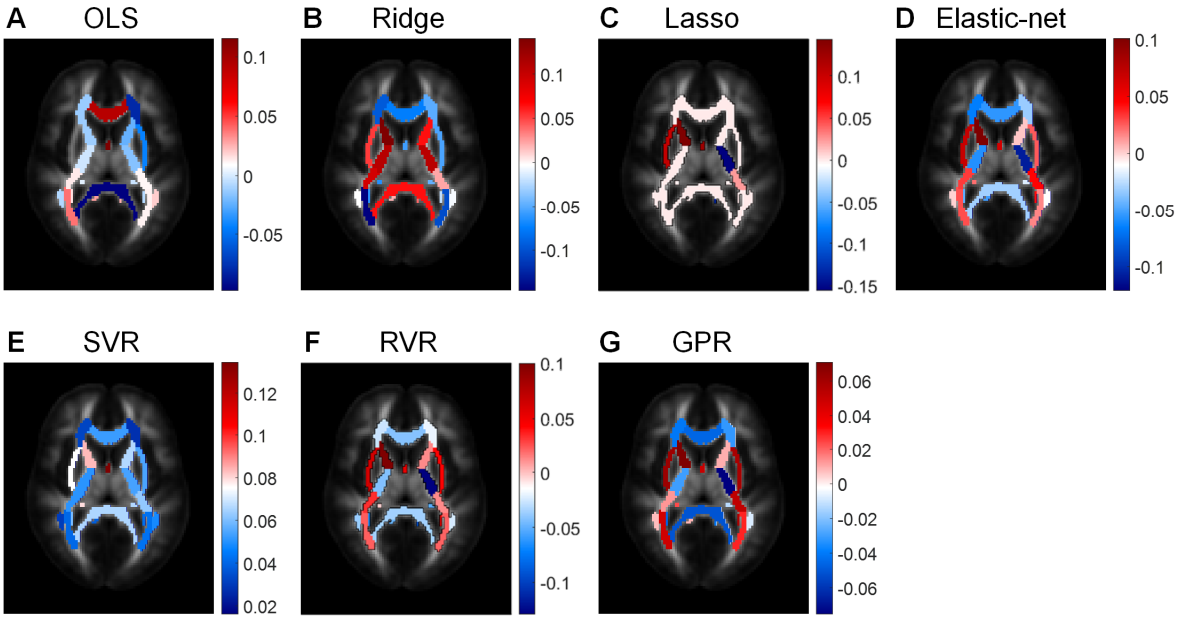

Supplementary Figure S6. A representative map of regression weights for axial diffusivity for brain-age prediction in Cam-CAN individuals in each of the seven

algorithms. OLS: Ordinary least squares regression; Lasso: Least absolute shrinkage and selection operator; SVR: Support vector regression; RVR: Relevance vector regression; GPR: Gaussian process regression.

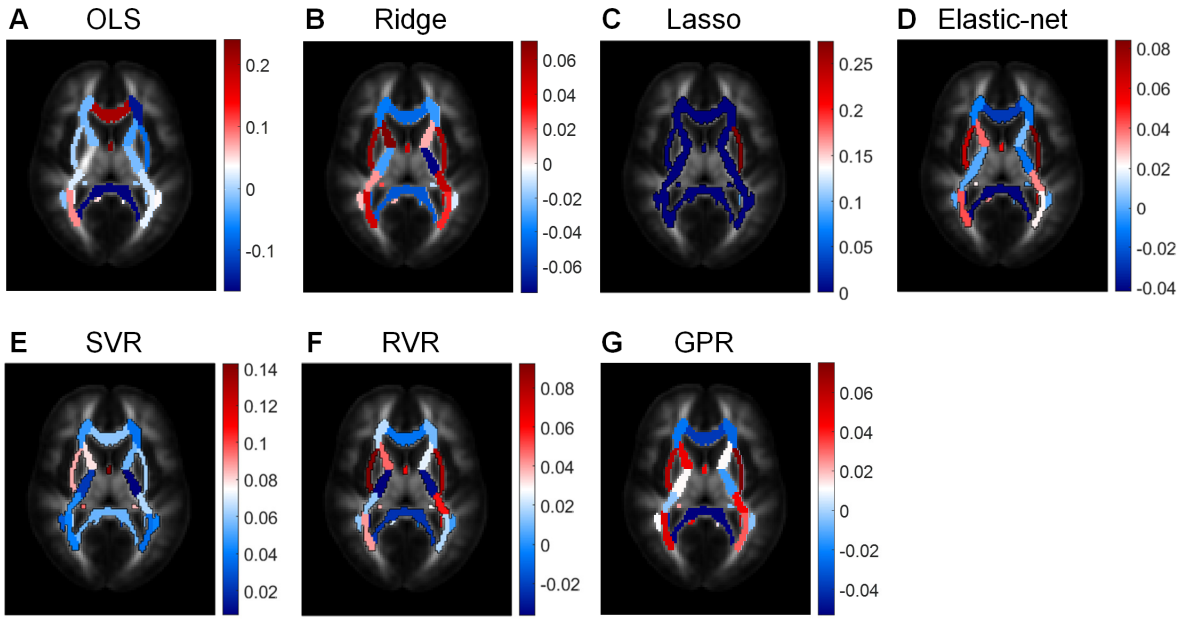

Supplementary Figure S7. A representative map of regression weights for radial diffusivity for brain-age prediction in Cam-CAN individuals in each of the seven algorithms. OLS: Ordinary least squares regression; Lasso: Least absolute shrinkage and selection operator; SVR: Support vector regression; RVR: Relevance vector regression; GPR: Gaussian process regression.

2. Computational speed of the algorithms

We assessed computational efficiency for each algorithm by recording the total computational time to train the model using 10-fold cross-validation on the training data. All models were trained on a machine with AMD Ryzen 9 5900X CPU and 32 GB RAM. Among algorithms, ridge regression was the fastest algorithm (0.06 s), whereas relevance vector regression was the slowest algorithm (3.56 s).

Supplementary Table S4. Comparison of computational speed of the algorithms for model training

Speed	OLS	Ridge	Lasso	Elastic-net	SVR	RVR	GPR
Training time (s)	0.58	0.06	0.34	0.34	0.29	3.56	0.31

OLS: Ordinary least squares regression; Lasso: Least absolute shrinkage and selection operator; SVR: Support vector regression; RVR: Relevance vector regression; GPR: Gaussian process regression.

3. Supplemental analyses for the association of brainPAD with cognitive function

Supplementary Table S5. Association of brainPAD with cognitive measures for each algorithm in the hold-out test set (N=101)

Algorithm	Catell's Fluid intelligence			Hotel			Proverbs			ToT			RT simple			RT choice			Emotion recognition		
	t	P_{FDR}	R	t	P_{FDR}	R	t	P_{FDR}	R	t	P_{FDR}	R	t	P_{FDR}	R	t	P_{FDR}	R	t	P_{FDR}	R
OLS	1.10	0.276	0.110	0.88	0.382	0.090	-0.10	0.918	-0.011	-0.48	0.630	-0.050	0.08	0.939	0.008	1.26	0.212	0.136	0.34	0.732	0.035
Ridge	-0.13	0.899	-0.013	-0.26	0.797	-0.027	-1.08	0.281	-0.110	0.84	0.403	0.086	-0.35	0.728	-0.038	0.62	0.534	0.068	-0.01	0.991	-0.001
Lasso	-0.01	0.990	-0.001	-0.03	0.972	-0.004	-0.99	0.326	-0.100	0.79	0.430	0.081	-0.72	0.476	-0.077	0.93	0.355	0.101	0.29	0.773	0.030
Elastic-net	-0.07	0.942	-0.007	-0.23	0.822	-0.023	-1.06	0.293	-0.107	0.87	0.389	0.089	-0.37	0.714	-0.040	0.67	0.505	0.073	0.04	0.968	0.004
SVR	-0.09	0.927	-0.009	0.03	0.978	0.003	-1.28	0.205	-0.129	0.92	0.361	0.094	-0.15	0.878	-0.017	0.92	0.362	0.099	0.29	0.773	0.030
RVR	-0.22	0.828	-0.022	0.07	0.945	0.007	-1.14	0.258	-0.115	1.26	0.211	0.129	-0.92	0.361	-0.099	0.25	0.800	0.028	0.23	0.816	0.024
GPR	-0.13	0.898	-0.013	-0.26	0.794	-0.027	-1.08	0.281	-0.110	0.84	0.403	0.086	-0.35	0.729	-0.037	0.62	0.535	0.068	-0.01	0.989	-0.001

None of the association between brainPAD and cognition variables was significant at FDR corrected p-value (P_{FDR}). OLS: Ordinary least squares regression; Lasso: Least absolute shrinkage and selection operator regression; SVR: Support vector regression; RVR: Relevance vector regression; GPR: Gaussian process regression.

Supplementary References

1. Segonne F, Dale AM, Busa E, Glessner M, Salat D, Hahn HK, Fischl B. A hybrid approach to the skull stripping problem in MRI. *Neuroimage* Jul 2004;22(3):1060-1075.

2. Fischl B, Salat DH, Busa E, et al. Whole brain segmentation: automated labeling of neuroanatomical structures in the human brain. *Neuron* Jan 31 2002;33(3):341-355.

3. Fischl B, Salat DH, van der Kouwe AJ, Makris N, Segonne F, Quinn BT, Dale AM. Sequence-independent segmentation of magnetic resonance images. *Neuroimage* 2004;23 Suppl 1:S69-84.

4. Sled JG, Zijdenbos AP, Evans AC. A nonparametric method for automatic correction of intensity nonuniformity in MRI data. *Ieee T Med Imaging* Feb 1998;17(1):87-97.

5. Fischl B, Liu A, Dale AM. Automated manifold surgery: Constructing geometrically accurate and topologically correct models of the human cerebral cortex. *Ieee T Med Imaging* Jan 2001;20(1):70-80.

6. Desikan RS, Segonne F, Fischl B, et al. An automated labeling system for subdividing the human cerebral cortex on MRI scans into gyral based regions of interest. *Neuroimage* Jul 1 2006;31(3):968-980.

7. Klapwijk ET, van de Kamp F, van der Meulen M, Peters S, Wierenga LM. Qoala-T: A supervised-learning tool for quality control of FreeSurfer segmented MRI data. *Neuroimage* Apr 1 2019;189:116-129.